Journal of Drug Delivery Science and Technology 60 (2020) 102043

Contents lists available at ScienceDirect

Journal of Drug Delivery Science and Technology

journal homepage: www.elsevier.com/locate/jddst

Research paper

Loading effects on the performance of needle-free jet injections in different skin models

Pankaj Rohilla [a], Idera Lawal [a], Andrew Le Blanc [a], Veronica O'Brien [b,1], Cormak Weeks [a], Whitney Tran [c], Yatish Rane [a], Emil Khusnatdinov [a], Jeremy Marston [a,*]

[a] Department of Chemical Engineering, Texas Tech University, Lubbock, TX, 79409, USA
[b] Margaret Talkington School for Young Women Leaders, 415 N Ivory Ave, Lubbock, TX, 79403, USA
[c] Department of Mathematics and Statistics, 1108 Memorial Circle, Lubbock, TX, 79409, USA

ARTICLE INFO

Keywords:
Jet
Needle-free
Viscosity
Transdermal

ABSTRACT

Intradermal delivery of vaccines with jet injection is one of the alternatives to conventional delivery techniques with hypodermic needles via the Mantoux technique and multi-puncture devices etc. However, for a given fluid, the effects of various parameters related to injector design, as well as skin properties are still not well understood. While the key design parameters are orifice diameter, jet speed, cartridge volume, and standoff distance, we must also consider the applied load of the device on the skin and axial skin tension. These parameters are all studied herein using different ex vivo models (guinea pig, pig, and human skin) and different fluid viscosities. We find that the applied load can have a significant effect on the amount of drug delivered through the skin, as well as the fluid dispersion pattern in the intradermal tissues. Regardless of skin type or fluid viscosity, we show that minimal standoff and applied force loads of approximately 1 kg (9.81 N) should be used to maximize injection efficiency when targeting intradermal tissue with the spring-powered device used in this study.

1. Introduction

Needle-free injector devices use impulse force for targeted vaccine delivery into the intradermal, subcutaneous, and intramuscular regions. Different actuation mechanisms such as spring force [1], Lorentz coil [2], compressed gas [3], piezoelectric motors [4], pyro-driven [5] and laser induced cavitation [6,7] have been used in the development of the needle free jet injectors, where the working principal is creation of a high-speed micro-scale jet that can puncture the skin and deposit drug into tissues beneath. To date, the clinical use of such devices has been limited, possibly due to a confluence of cost, pain, bruising, and inefficient delivery of the vaccine [8,9]. Other needle-free drug delivery techniques include microneedles [10], topical solutions [11], iontophoresis [12] and powder injections [13] etc. However, such alternative transdermal drug delivery techniques are limited by poor delivery control, limited dosage, and high cost [14,15]. The advent of high-immunogenicity DNA-based vaccines and the need for high force to deliver such viscous products has increased interest in improving the design of jet injector devices [16,17]. It is also noted that jet injections result in higher absorption rates as compared to needle injections due to the formation of more diffused dispersion patterns inside the skin [1].

The major challenges in the development of the jet injectors are inefficient delivery (percentage of expelled drug actually delivered across the skin) and controllability of the depth, which is especially relevant in targeted vaccine delivery. To combat this, various design parameters such as orifice diameter, cartridge volume, standoff distance, viscous losses in the nozzle, and jet speed profile have been studied in the literature [2,18,19]. The physical properties of the vaccine and mechanical properties of the skin also affect the delivery efficiency and the dispersion of the drug inside the skin [20,21].

In general, a jet injector is placed perpendicular to the skin, but can also be placed at an angle to deliver a drug [22,23]. Whilst the effect of placement of the jet injector on the delivery performance is unclear, the original observations of Hingson & Hughes [24] indicated that an offset resulted in some intradermal accumulation. As such, a spacer ring in contact with skin can be used to provide a stand-off distance between the orifice and the skin, and to keep the jet injector in a fixed position [25]. However, in the act of keeping the jet injector on the skin, a force of

* Corresponding author.
E-mail address: jeremy.marston@ttu.edu (J. Marston).
[1] Current Affiliation: Department of Biology and Biochemistry, University of Houston, Houston, Texas 77004.

https://doi.org/10.1016/j.jddst.2020.102043
Received 21 May 2020; Received in revised form 26 August 2020; Accepted 26 August 2020
Available online 6 September 2020
1773-2247/

different magnitude is applied, depending on the individual administering the injection. The nature of the applied force is both compressive and tangential, which results in additional tension across the skin and stress in the tissue beneath the skin. The biaxial stiffness properties of skin tissues have been measured in the past by applying a force in-plane, out-of-plane, and normal deformation to the skin tissues [26].

While the effect of this applied load on transdermal drug delivery has not been systematically investigated before, we note that needle-free injection devices have been modified with a force sensor [22] or designed specifically to pre-tension the skin using either a threshold applied normal load [27], or a nozzle device to stretch the skin axially before actuating the jet [28]. In this article, we have therefore attempted to quantify the effect of applied loading on the performance of the jet injections in addition to other parameters such as standoff distance, liquid viscosity, cartridge volume, orifice diameter, skin type (animal) and skin support (underlying tissue).

The availability and cost of human skin limits its use in drug delivery studies. Thus, various skin models such as rodent and mammalian skin have been used to mimic human skin behavior in the literature [29]. If fresh human skin is not easily available, it has been reported [30] that fresh porcine skin at high humidity conditions can be used as a suitable substitute. It should be noted that in the cited study [30], miniature Yucatan pigs were used, which can have different and unfavorable mechanical properties as a skin model to human skin when compared to the pig breeds raised for commercial meat production. In this study, we have used porcine skin, guinea pig skin and human skin to inject liquids with jet injectors. Delivery efficiency and aspect ratio of dispersion pattern formed by the liquid under the skin were used to characterize performance. For porcine tissue, injections into skin on cadavers as well as freshly excised and frozen skin parts of the same cadavers were performed.

We have both qualified and quantified the effect of a wide range of variables associated with the skin, injector device and the fluid viscosity on the jet injection delivery. The results presented aid in better understanding of these parameters to overcome the current challenges in the development of needle-free jet injector devices.

2. Methods

Skin samples: Porcine, Guinea pig skin, and human skin were procured from Animal Sciences (Texas Tech University), Inovio Pharmaceuticals, and National Disease Research Interchange (NDRI), respectively, and all had thicknesses around 3–5 mm. Guinea Pig skins were kept in a freezer at −4 °C whereas human skin and porcine skin were stored in a freezer at −20 °C. In addition to injections performed on cadavers, the porcine skin was harvested from Yorkshire-Cross pigs euthanized at 13 weeks of age in the animal science building. Human skins used were from Caucasian males and females in the age range of 55–81 and with BMI indexes ranging from 21.50 to 29.86 (see Table S14). It should be noted that the majority of vaccines are delivered at an early age, whereas the age range used in our study is significantly older, and might not reflect similar mechanical properties of human skin at a young age.

Skin supports: To mimic different tissues beneath the skin samples, we used either (a) rigid glass substrate, (b) 1 cm lean porcine tissue, (c) 2 cm lean porcine tissue, or (d) 1 cm porcine fat layer. All porcine tissue used for supporting human and GP skin was procured from a local butcher and was frozen at −4°C. The skin and pork meat were thawed to room temperature before the injection.

Device and loading protocol: A spring-powered device (Bioject ID Pen) was used to perform jet injections, which ejects a volume, V, of either 50 μl or 100 μl from a rigid plastic cartridge. The cartridge tip is circular with diameter of ≈ 3.5 mm, and the orifice diameter, d_o, was either 155 or 175 μm. To achieve a range of the stand-offs, S, of either 0, 2 or 14 mm, an annular spacer ring (≈ 16 mm in diameter) is attached to the nozzle. DI water and 80% glycerol were used as injectate liquids due to their viscosity gap of nearly 2 orders of magnitude with μ of 1 mPa s and 84 mPa s, respectively. Once loaded with a filled cartridge, the jet injector was firmly fixed onto a vertical stage with uniaxial motion, and lowered onto the skin sample, which was kept on a mass balance to register the applied normal load. The value of normal load could then be varied simply by adjusting the vertical position of the injector. In addition, a miniature load cell (Futek - LLB 130, 50 lb, Item #FSH03880) was embedded within the mass balance to provide more detailed measurement of the injection force at a sample rate of 4800 sps (see Fig. 1 (a)). Applied normal load, L_n, on the skin was observed visually from the mass balance and was varied from $0 - 2$ kg, which translates to a normal force of 0–19.62 N. Fig. 1(b) and (c) shows the loads applied (L_n and L_a) and the deformation of the skin when a normal force of 9.81 N is applied by a jet injector. To achieve axial loading, L_a, skins were sewed on two sides with one side fixed on a post and the other side attached to a hanging load of either 0.5 kg (4.9 N) or 1 kg (9.81 N). The axial loads were chosen to compare the effect of similar loads when applied in axial or normal direction on the skin. To avoid structural damage to the skins, axial loading was limited to the maximum hanging load of 9.81 N.

Imaging and characterization: To visualize the dispersion of liquids into the skin, Trypan Blue (Sigma Aldrich) was added to the liquids used for the injection concentration of 1 mg/ml. After injection, skins were frozen to −4°C, and then cut along the cross-section of the injection site to visualize the intradermal bleb, whose dimensions (total depth, h, width, w, and depth at maximum width, d) were measured using image processing in Matlab (see Fig. 3 for an example). We then characterize the dispersion pattern with aspect ratio $AR = d/w$. To characterize efficiency of the delivery (η), we used a volume-based measurement, given by the ratio of fluid injected across the skin to that ejected by the device as:

$$\eta = \frac{\left(\rho V_{ej} - m_{rejected}\right)}{\rho V_{ej}} \times 100 \quad (1)$$

Efficiency of delivery into the intradermal tissue can be overestimated as liquid can accumulate and diffuse into the subcutaneous region as well. Thus measurement of mass alone does not necessarily reflect just the intradermal accumulation. Imaging (as in Figs. 3–6) can provide additional information about the extent of liquid, but again may reflect diffusion that occurs post-injection. As such, in the present study, it is difficult to compare performance of jet injection technique with Mantoux technique in terms of the bleb volume and injectate retained within different regions of skin. However, using micro-computed tomography (μCT) can be useful in this regard [31] and will be pursued in future studies.

For each individual configuration of human skin, a minimum of 10 replicates were done, whereas for guinea pig and porcine skin, a minimum of 5 replicates were done. The statistical significance of the different parameters (e.g., L_n, L_a, μ, d_o, V, S, skin type etc.) on both AR and η was determined by ANOVA tests with significance level $\alpha = 0.05$.

3. Results and discussion

i. Applied loading

Skin is a viscoelastic material which shows relaxation when stretched and kept at a constant strain [32]. Pressing a jet injector with a spacer ring results in a compression force on the skin as well as tangential stress within the skin, as shown in Fig. 1(b). The behavior of the skin has been seen to be dependent on the load history; Cyclic loading in a nonlinear fashion yields a shift in stress-strain curves until a convergence [32]. We therefore also studied the effect of load history by using three different loading mechanisms.

In the loading mechanism type A, the jet injector was initially pressed on the skin with an extra ≈50% of the target load (i.e. $L_o \approx \frac{3}{2}L_n$).

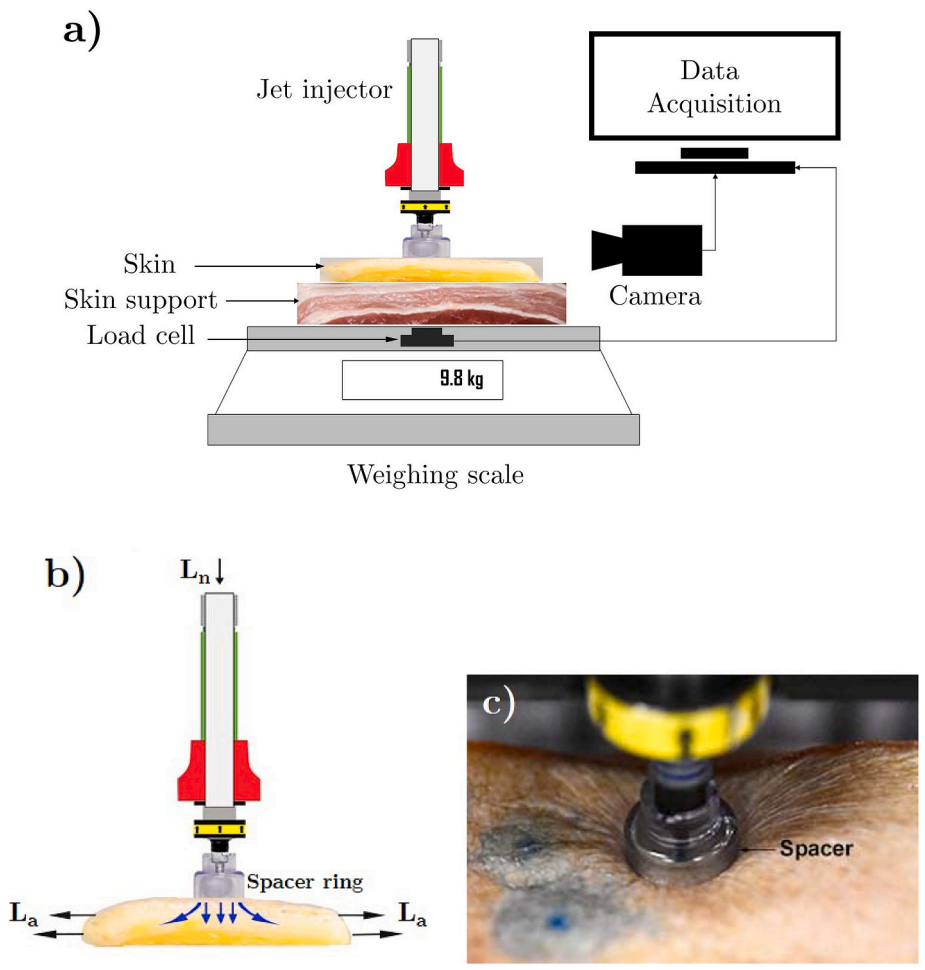

Fig. 1. Experimental. **a).** Schematic of the experimental setup, **b).** Schematics of applied normal load, L_n and axial load, L_a, both shown by black arrows, and hypothesized distribution of stress in the skin tissue shown by blue arrows and **c).** Human skin under tension by a spacer ring with an applied normal force load of 9.8 N by jet injector. (For interpretation of the references to colour in this figure legend, the reader is referred to the Web version of this article.)

As observed from the weighing balance, the load on the skin decreases non-linearly due to the skin relaxation in which the applied load distributes itself within the skin layers. An example of the loading profile, as determined by the high-resolution load cell, for type *A* mechanism for $L_n \approx 4.9$ N on guinea pig (GP) skin is presented in Fig. 2. Here, the injector was loaded onto the skin at a normal load of ≈750 g corresponding to a force of ≈7 N. The applied load decreases due to the skin relaxation and the jet injection was actuated once the load reaches a value of ≈ 4.9 N. Injection duration can be seen in the figure as a spike in the force. Although the increase in force during jet injection was observed to be in the order of ≈ 4 N, this is due to the extra manual force exerted during triggering; The actual force profile for jet injection (without any manual force) with similar nozzle and liquid parameters was reported in our past work [33] and is of order of 1 N.

In type *B* mechanism, the skin was loaded by extra ≈50% weight followed by relaxation to the required weight for 2 cycles. The injection was then triggered when the weight approaches the required loading value in the second cycle. Lastly, Type *C* mechanism is identical to type *A* mechanism except for the initial loading weight (L_o), which was chosen to be twice as that of the required value of the load i.e. $L_o = 2L_n$.

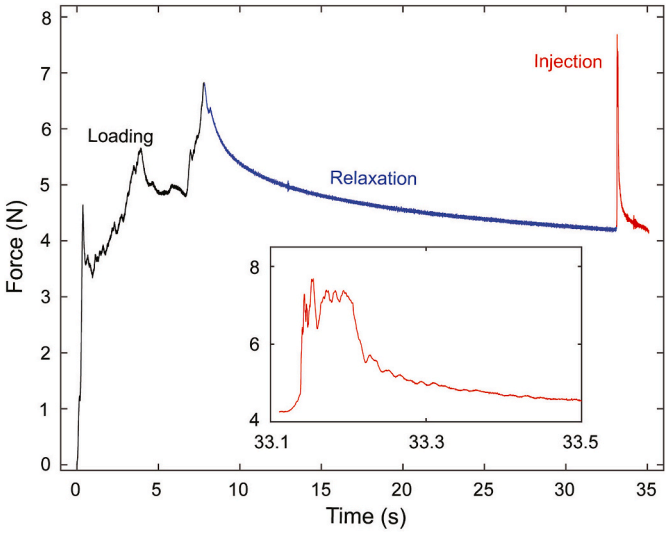

Fig. 2. Force measured by the load cell underneath the weighing balance plate for 80% glycerol solution injected through a nozzle with an orifice diameter of 155 μm into the GP skin with $S = 0$ mm and $L_n = 4.9$ N. The different stages in the force profile include (*i*) the loading stage, (*ii*) the relaxation stage and (*iii*) the jet injection stage. Inset shows the force profile during jet injection.

ii. Liquid dispersion

The depth and shape of the bleb (i.e., fluid distributed within the intradermal tissue) ultimately dictate the effectiveness of delivery and the diffusion of the vaccine within the skin. Liquid dispersion inside the

skin was characterized by the aspect ratio of the bleb formed in the skin, i.e. $AR = d/w$, as shown graphically in the example in Fig. 3. One would intuitively expect fluid dispersion in the intradermal tissue to be affected by various parameters such as viscosity and mechanical properties of the skin (e.g. skin type and applied load). However, orifice diameter and standoff distance affect both the impact velocity and impact footprint of the liquid jet [33], and therefore it is instructive to examine these effects as well. As a brief overview, cross-sections of blebs formed after jet injection into the different skin types, under similar conditions are presented in Fig. 4.

The effect of increasing applied load caused by the hollow cylindrical spacer creates an extruded dome shape on top of the skin, which becomes more defined with increased load, as can be seen in Fig. 5. However, the bleb shape under the skin also changes from an oblate ellipsoidal to cylindrical shape with increase in the normal static load, as seen in Fig. 6. That is, the bleb width increased as the applied normal load was increased to 19.62 N. This can be understood by considering the compressed state of the skin when under load; the compressive stress in the skin and intradermal tissues leads to axial bias for dispersion, resulting in fluid being squeezed farther in the horizontal direction.

In addition to the static load, the effects of standoff and fluid viscosity assessed previously [21] are also hypothesized to become important due to their respective influences on the jet impact footprint and diffusion coefficient in porous substrates. Indeed, increasing standoff distance from 0 mm to 14 mm also showed transition to cylindrical shape of the skin bleb. However, blebs formed from 14 mm standoff were narrow in width with higher aspect ratio as compared to injections from zero standoff distance. A comparison of aspect ratio, AR, of the blebs formed inside the GP skin for different standoff, applied normal load and injectate viscosity is presented in Fig. 7, where the most significant variation occurs for $L_n = 9.81$ N, but in all cases, increasing the standoff distance increased AR accordingly.

Complete analysis for all skin types shown in Supplemental Figs. S3, S4, and S5 corresponding to guinea pig, porcine, and human skins. However, two key observations that must be highlighted are for the porcine skin (Fig. S4), where we were able to compare freshly excised skin to skin having undergone a single freeze-thaw cycle; For injection into the ventral region of skin, the bleb shape changed significantly from fresh ($AR \approx 0.5$) to frozen-thawed ($AR \approx 0.24$). However, the same injections into dorsal skin were invariant to the freeze-thaw cycle with $AR \approx 0.1$ in all cases (see Fig. S4b). Furthermore, for the freshly excised skin, the effect of orifice diameter was also significant for both viscosities (see Fig. S4a), where $AR \approx 0.25$ for $d_o = 155$ μm, but $AR \approx 0.1$ for $d_o = 175$ μm.

ii. Delivery efficiency

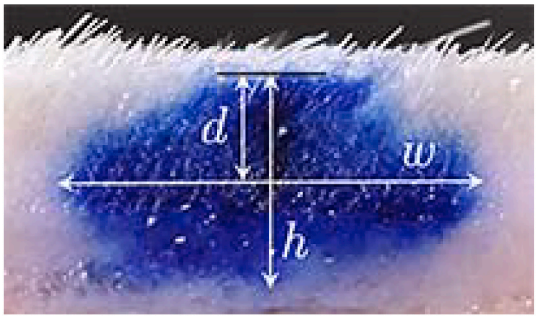

Fig. 3. The dimensions of the bleb formed inside the skin after jet injection. W is the maximum width of the bleb, h is the total depth of the bleb from the surface of the skin, and d is the distance between the depth at the maximum width of the bleb and the surface of skin.

3.1. Porcine skin

In this study, we have used three different states of the porcine skin including cadaver, freshly excised, and frozen skin. Liquid was injected into the cadavers within an hour of euthanasia such that injections were performed with minimum alteration in skin mechanical properties. Furthermore, skin from different anatomical parts including ventral and dorsal parts was also excised and used both before and after a cycle of freezing and thawing. The mechanical properties of porcine skin after a single cycle of freezing and thawing are nearly the same as that of human skin [30]. However, the ventral porcine skin is known to be more anisotropic in comparison to the dorsal part [34]. Although various properties of porcine and human skin are similar, such as morphology, immunogenicity, physiology, and composition of cells; mechanical properties of the top layer of the skin, i.e. stratum corneum (SC) are different. Porcine SC exhibits higher Young's modulus (E_{SC}) than human skin, which increases further after a freeze-thaw cycle, whereas a decrease in the E_{SC} was observed for human skin after a freezing cycle [30].

3.2. Load

No significant effect of applied load was observed on the delivery efficiency of the injectate inside the freshly excised porcine skin ($p > 0.05$ as per Table S9). However, large intrasample variation (η in the range of 11%–53%) was observed for the normal force of 9.81 N as shown in Fig. 8(a). The delivery efficiency of the jet injection was calculated on the basis of liquid left on the top of the skin after the jet injection, as per Eq. (1).

3.3. Viscosity

For water injected into fresh porcine skin, the delivery efficiency was $\eta \approx 20 - 40$ %, as shown in Fig. 8(a). However, by increasing the fluid viscosity (by nearly an order of magnitude) - we observe lower η for 80% glycerol in comparison to that obtained with DI water for an applied normal force of 9.81 N.

3.4. Standoff distance

Three different standoff distances ($S = 0$, 2, 14 mm) between the nozzle orifice exit and the fresh dorsal skin were used. A reduction in the percentage delivery was observed with increase in the standoff distance from 0 mm to 2 mm as shown in Fig. 8(a). Whereas the best overall performance in terms of highest efficiency was observed for $S = 0$. There was large intrasample variation in the data for standoff distance, rendering the effect of S on η insignificant ($p > 0.05$) for fresh skin.

3.5. State of the skin

The anatomical location of the skin and its state (fresh or frozen-thawed) are important for determining the mechanical properties of the skin, and therefore should affect the volume that can be delivered within the skin. A summarized comparison is presented in Fig. 8(b), where we found nearly complete delivery ($\eta \geq 95\%$) was achieved for injection of $V = 50$ μl water in the freshly excised skin from the ventral region. However, efficiency decreases significantly for $V = 100$ μl to $\eta \approx 20 - 30\%$. In contrast, delivery efficiency in the dorsal skin was low in both cases ($\eta \approx 15\%$ and 5% respectively). Porcine skin showed higher delivery efficiency in the dorsal part of the skin after a cycle of freezing and thawing. On the other hand, the ventral part of the skin after a freeze-thaw cycle showed lower injection efficiency in comparison to the fresh skin. Nearly complete delivery of 50 μl water in freshly excised skin from ventral part is an exception case of high percentage delivery. This exception can be attributed to the highly localized variability in the mechanical properties of the porcine skin. In contrast, the higher

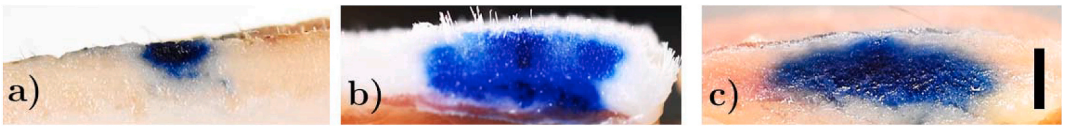

Fig. 4. Cross-sectional view of the blebs formed by dyed water injected into (a) porcine skin, (b) guinea pig skin and (c) human skin. Skin bleb shown here corresponds to d_o = 155 μm, S = 0 mm, and L_n = 9.8 N. *Scale bar represents* 5 mm.

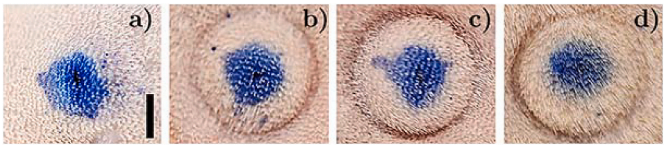

Fig. 5. Effect of applied load on GP skin (top view) supported by a layer of lean pork meat (*thickness* = 2 cm) after a jet injection of dyed water through a nozzle with an orifice diameter of 155 μm for (a) L_n = 0 N, (b) L_n = 4.9 N, (c) L_n = 9.8 N and (d) L_n = 19.6 N. *Scale bar represents* 5 mm.

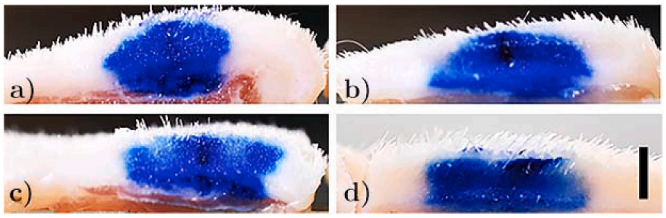

Fig. 6. Cross-sectional view of the blebs formed in the GP skin supported by a layer of lean pork meat (*thickness* = 2 cm) injected with dyed water (V = 100 μL) through a nozzle with orifice diameter of 155 μm for (a) L_n = 0 N, (b) L_n = 4.9 N, (c) L_n = 9.8 N and (d) L_n = 19.6 N. *Scale bar represents* 5 mm.

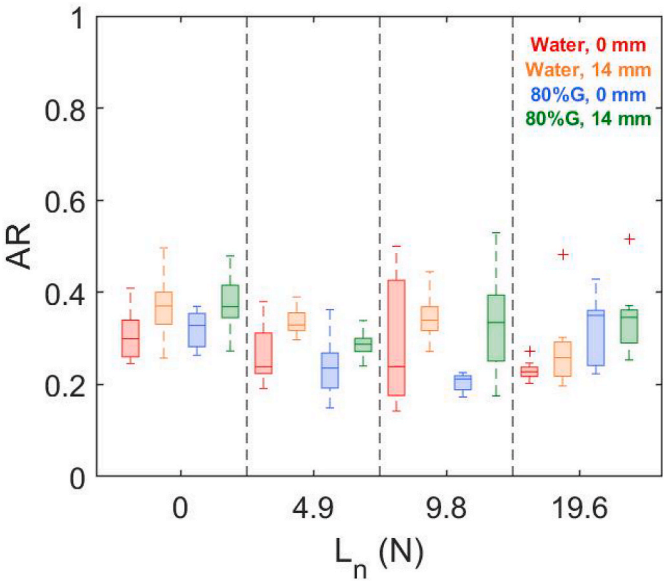

Fig. 7. Comparison of aspect ratio (AR) of the blebs formed in GP skin supported by a layer of leaned porcine meat (*thickness* = 2 cm) for different L_n, s and μ. (d_o = 155 μm, *Mean ± Standard Error*, n = 5).

delivery in frozen porcine skin from dorsal region can be attributed to higher diffusivity as compared to the fresh skin. Increase in diffusivity of the skin from fresh to frozen is due to the increase in porosity from structural damage as the freezing induces formation of the ice crystals within the skin [35].

Porcine cadavers were also injected with water into different parts corresponding to the different mechanical properties (Thigh, Dorsal, Side, Ventral). The effect of variation in anatomical parts on the injection delivery efficiency was very significant ($p < 0.05$), with higher efficiency observed for the ventral skin followed by side skin, dorsal skin and thigh skin as shown in Fig. 8(c). Thus, percentage delivery via jet injection was observed to be inversely proportional to stiffness of the porcine skin.

One interesting comparison can be made between our results herein and those of ref [22], who also used thawed porcine skin with applied forces of 0–8 N (equivalent to applied loads of 0–0.82 kg). Their results showed a delineation for forces 0–3.9 N and 4–8 N, with a marked increase in delivery efficiency ($\eta \approx 90\%$) for the higher force range. Their results (on porcine tissue) do not correspond to our results for porcine tissue, which could be due to a number of reasons such as device configuration, type of pig breed and anatomical location of the skin harvest. However, their observed delivery efficiencies are better reflected by our results for human skin (see below in Fig. 10).

3.6. Guinea pig skin

Guinea pig skin was also used as a surrogate for human skin. For these trials, we also used axial loading (L_a) in addition to normal force loads (L_n) of 0, 4.9, 9.81 and 19.62 N. Variation in the thickness of subcutaneous and muscular layers of the skin was mimicked by supporting the GP skin with leaned porcine meat of different thickness of 1 cm and 2 cm and a fat layer of 1 cm in thickness. In addition, a rigid support (glass slab) was used to mimic the skin supported by the bone in case of axial loading experiments.

As shown in Fig. 9(a), GP skin supported by 2 cm porcine meat exhibited significant effect of applied normal load on the delivery efficiency of water and 80% glycerol ($p < 0.05$) for standoff distance of 0 mm. However, the effect of L_n was insignificant ($p > 0.05$) for jet injection from the standoff distance of 14 mm for different injectates. A normal load of L_n = 9.81 N resulted in the highest delivery efficiencies with $\eta \geq 95$ % for water and $\eta \approx 75\%$ for 80% glycerol, as shown in Fig. 9(a). However, further increasing the normal load to L_n = 19.62 N resulted in lower delivery efficiency of both liquids. A similar effect of L_n on injection efficiency was observed for the GP skin on different underlying supports (see Fig. S2). Again, we can interpret this result in the context of tension and stress within the intradermal and underlying support tissues; for low loads ($L_n < 4.9$ N), the underlying support is still pliable so that it can deflect due to the impulsive action of the jet. At high loads $L_n \geq 19.62$ N, the underlying support is compressed and stiff, and the intradermal tissues are also under significant compressive stress, resisting liquid dispersion throughout the injection. Therefore, the value $L_n \approx 9.81 - 19.62$ N represents a near-optimal trade-off between these two regimes which removes the influence of underlying tissue, but also correctly tensions the skin for puncture and liquid dispersion.

Axial load was applied in addition to the normal static load to understand the effect of additional tangential forces within the skin. Fig. 9 (b) shows the effect of different magnitudes of loading on the injection efficiency of the dyed water inside the GP skin supported by glass or leaned pork. With fixed axial loading (L_a) of 4.9 N on GP skin supported by 2 cm thick lean pork, the effect of L_n on η was significant ($p < 0.05$). However, when compared to the results in Fig. 9(a), it is clear that addition of axial load is detrimental to injection efficiency, since $\eta|_{L_a=0} \geq 80\%$ but $\eta|_{L_a=0.5} \leq 40\%$. We propose that axial load , in addition

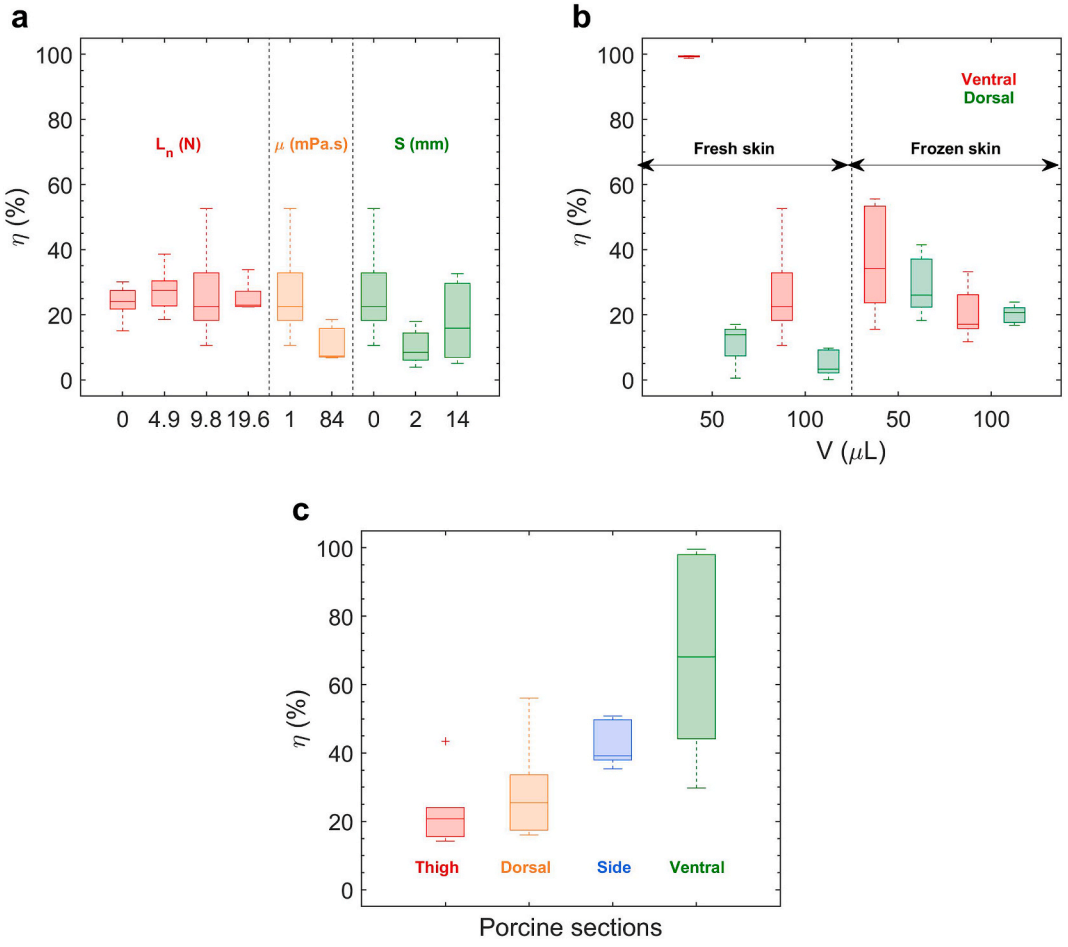

Fig. 8. Injection efficiency (η) for jet injections into porcine skin. **(a)** The effect of normal force load (L_n), liquid viscosity (μ) and standoff distance (S) on delivery efficiency of the liquid in a freshly excised porcine skin ($d_o = 155$ μm). **(b)** The effect of the state of skin (*fresh or used after a single freeze-thaw cycle*), region of skin (*ventral or dorsal)* and the target volume on the delivery efficiency for dyed water injection into porcine skin ($d_o = 155$ μm and $S = 2$ mm.) **(c)** Delivery efficiency for dyed water injection into thigh, dorsal, side, and ventral regions of porcine skin ($d_o = 155$ μm and $S = 2$ mm). (*Mean ± Standard Error, n = 5*).

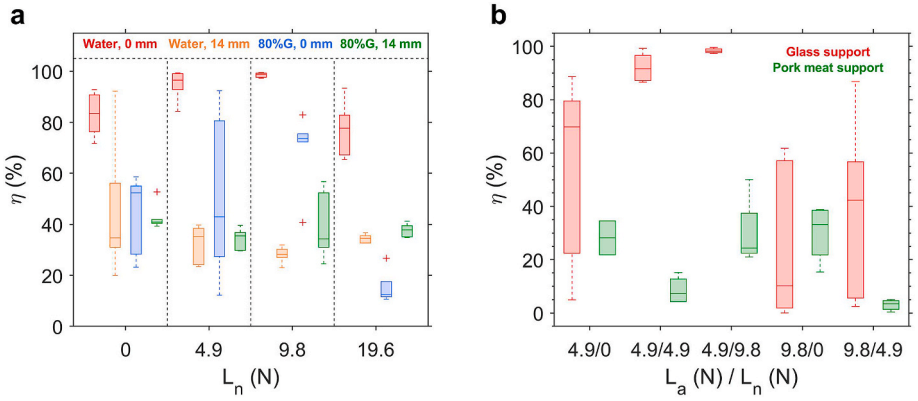

Fig. 9. Injection efficiency (η) for jet injections into guinea pig skin. (a) The effect of normal force load (L_n), standoff distance (S), and injectate viscosity (μ) on η for GP skin supported by a layer of lean pork meat (*thickness* = 2 cm) and **(b)** The effect of axial force load (L_a), normal force load (L_n), and the skin support on η for dyed water injection ($S = 0$ mm and $d_o = 155$ μm). (*Mean ± Standard Error, n = 5*).

to normal load, results in excessive stress within the skin, which does not allow for fluid accumulation from the incoming jet flow.

In case of higher axial load of 9.81 N, GP skin is even more highly tensioned and addition of normal load resulted in lower injection efficiency. The overall effect of axial loading with constant normal static load either showed insignificant effect or a lower injection delivery. Therefore, the results for GP skin advocate that an optimal configuration exists. For GP skin, this configuration is: $S = 0$ mm, $L_n = 9.81$ N, $d_o = 155$ μm, and 2 cm thick underlying tissue.

3.7. Human skin

Human skin varies in terms of mechanical properties with age, loading, and different anatomical regions [36–40]. The elastic modulus

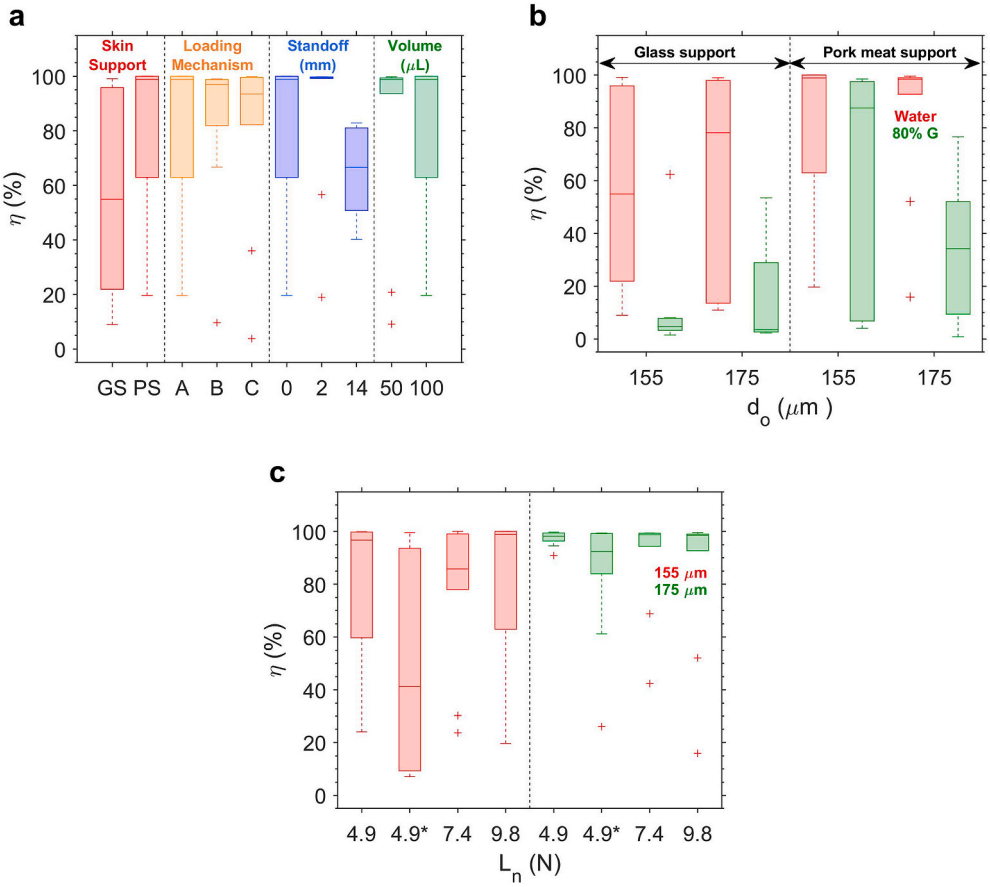

Fig. 10. Injection efficiency (η) for jet injections into human skin. **(a)** The effect of skin support (i.e., glass support (*GS*) or porcine meat support (*PS*)), loading mechanism, standoff distance and injectate volume on η for $L_n = 9.8$ N, **(b)** The effect of d_o, skin support and injectate viscosity (μ) for $S = 0$ mm, **(c)** The effect of d_o, L_n and L_a on η for 2 cm porcine tissue support with $S = 0$ mm (**represents additional axial force load of 4.9 N using hooked weights*). (*Mean ± Standard Error, n = 10*).

of human skin increases with aging in addition to significant variation in thickness, stiffness, and tension [41] Behavior of human skin is visco-elastic in nature and the mechanical response to loading depends on the support or the backing material. After loading, relaxation occurs faster for skin over the muscle in comparison to the skin supported by the bone. Moreover, the skin over the muscle can tolerate higher applied load as compared to the skin supported by the bone [42]. We have used porcine tissue and glass slab as the backings underneath human skin to understand the effect of stiffness of the skin support on jet injection with applied load. Different loading mechanisms, standoff distances, and cartridge volumes were used to compare the efficiency of injection for a constant normal static load of 9.81 N as shown in Fig. 10(a).

For 100 μl water injection in human skin supported by glass slab, a large variation in percentage delivery was observed (η ≈20→95%). Whereas injection in human skin supported by porcine tissue yielded higher efficiency (η > 60%). Since applied loading is known to alter the structure and distribution of the forces within the skin layers, we used three different types of loading mechanisms (*A*, *B* and *C*). Type *B* and type *C* loading mechanism leads to high injection efficiency ($\eta > 80\%$) with small intrasample variation. However, skin stays under compression for longer time duration for loading mechanism type *B* and type *C*, which could challenge tissue integrity and, from the perspective of clinical implementation, are impractical. Standoff distance ($S = 0$ mm, 2 mm and 14 mm) was a highly significant factor for human skin injections, with $S = 2$ mm water was completely delivered within the skin followed by delivery efficiency obtained with water injected at $S = 0$ mm. Whereas, higher standoff distance of 14 mm showed lower injection efficiency. The effect of cartridge volume was also significant, with nearly complete delivery of $V = 50$ μl, but reduced efficiency for $V = 100$ μl with large intrasample variation. This indicates that there can be a limit in terms of deliverable volume ($50 \leq V_c < 100\mu l$) for jet injection, which should not be exceeded to reduce wasted products and cross-contamination from rejected fluid. It should be noted that jet injection is not the only technique limited by the lower percentage delivery of a drug with a volume of 100 μl. The loss in volume delivered can also be observed in other techniques like Mantoux injection. The deliverable volume by a single injection depends on the local capacity of the skin and the rate of drug delivery.

Orifice diameter, viscosity of the injectate and the skin support showed significant effect on the delivery efficiency as presented in Fig. 10(b). The effect of injectate viscosity was very significant ($p < 0.05$) regardless of the skin support with an exception of injection via nozzle with $d_o = 155$ μm into human skin supported by pork tissue ($p > 0.05$). The dyed water showed higher delivery into human skin in comparison to 80% glycerol injection. In addition, the effect of orifice exit diameter of nozzle on percentage delivery was not significant ($p > 0.05$) for different injectates and different skin supports.

The dual effect of applied load and orifice diameter is presented in Fig. 10(c), which indicates that a load of $L_n \approx 4.91$ N with an orifice diameter of 155 μm provides the optimal configuration for loading mechanism type *A* (the most practical of the three) with $S = 0$ mm. As with GP skin, addition of axial skin tension is deleterious when used in combination with applied load.

4. Conclusions

In this study we examined jet injection into freshly excised skin and skin that had undergone freeze-thaw cycle. One of the key factors for this

study was that of applied load, as well as device parameters such as orifice diameter, standoff distance, ejected volume and fluid viscosity. It should be noted that our study was conducted in the context of intradermal delivery targeting a volume of 100 μL.

The bleb (fluid distribution pattern) formed in the intradermal tissues showed some qualitative variation in terms of overall shape, but across a wide range of parameters, we did not find statistically significant effects. As such, the principal metric we focused on was delivery efficiency, i.e. the ratio of liquid deposited under the skin to that ejected from the injector.

Nearly complete delivery of water was obtained for GP skin supported by lean pork when a normal load of 9.81 N was applied. We hypothesize that this load represents a near-optimal load that removes the compliance of the underlying tissue and correctly tensions the skin, but does not result in excessive compressive stress within the intradermal tissues. This is supported by results at higher normal loads (L_n = 19.62 N) or those with added axial load, which showed reduced efficiency.

Anatomical variation of mechanical properties of skin was best highlighted using porcine skin, where we performed injections into cadavers, as well as freshly excised skin. In both cases, the highest injection efficiency occurred into ventral region skin, and we noted that injections with $V = 50$ μl in fresh skin also achieved near-complete delivery (≈ 100%). After a single freeze-thaw cycle, the same configuration performed poorly with lower percentage delivery of $\eta < 55\%$. The other configurations exhibited nearly similar or slightly higher efficiency after a single freeze-thaw cycle, which we attribute to local structural damage caused by ice crystals.

In human skin, we used different loading protocols and found that a two-cycle loading (type *B*) showed higher delivery efficiency. Increasing standoff to 14 mm showed low delivery efficiency. As with porcine skin, a lower injectate volume ($V = 50$ μl) showed nearly complete delivery into the human skin as compared to 100 μl, where the percentage delivery varied from ≈60% to ≈100%. Additional axial loading also led to poor injection efficiency for human skin.

In summary, applied load, liquid properties, nozzle geometry, and mechanical properties of the skin can strongly affect the delivery via jet injection, and the principal effect of these parameters is shown in Table 1. Furthermore, the optimal configurations for different skins for this ID pen device are presented in Table 2, which shows that $S = 0$ mm, $d_o = O(100)$ μm, $L_n = 9.81$ N, $V = 50$ μl is an all-round optimal configuration, other factors notwithstanding. Whilst these settings are specific to this device, they may be useful to help guide development of other jet injectors.

The state of the skin (both the tension of the stratum corneum and the stress within the dermal tissue) is clearly paramount for successful jet injection. Namely, the compressive (normal load/normal force) stress must be above a threshold value, whilst the in-plane (axial load/lateral force) stress should be minimized in order to allow the injectate to flow within the dermal tissue, which is a poro-elastic matrix. A precise understanding of the flow physics within the dermal tissues during jet injections is still lacking and must be pursued with a combined experimental-numerical approach.

Author contributions

P.R. and **J.M.** conceived the project and designed the experiments. **A.L.B.**, **I.L.** and **P.R.** performed the experiments on the guinea pig skin. **V.O.B.**, **C.W.**, **W.T.**, **I.L.** and **P.R.** performed the experiments on the human skin. **C.W.**, **E.K. I.L.** and **J.M.** did the experiments on the porcine cadavers and excised the skin from the cadavers. **Y.R.** contributed in experiments on the GP skin with 19.62 N normal static load. **P.R.** analyzed all the data and wrote the manuscript with **J.M.**

Table 1
Summary of effect of parameters on delivery efficiency of the jet injections (*decreases after $L_n = 9.81$ N).

	Guinea Pig skin	Porcine skin	Human skin
S, mm	↓	↓	↑↓
d_o, **μm**	–	–	↑
L_n, **N**	↑*	–	↑
L_a, **N**	↓	–	↓
V, **μl**	–	↓	↓

Table 2
Optimal configuration for jet injections in different skin models.

	Guinea Pig skin	Porcine skin	Human skin
S, mm	0	0	2
d_o, **μm**	155	155	155
Loading mechanism	–	–	*B*
L_n, **N**	9.8	9.8	9.8
L_a, **N**	0	–	0
***V*, μl**	50	50	50
Skin support	2 cm thick lean pork	–	2 cm thick lean pork

CRediT authorship contribution statement

Pankaj Rohilla: Formal analysis, Data curation, Writing - original draft, conceived the project and designed the experiments, performed the experiments on the human skin, analyzed all the data and wrote the original draft manuscript. **Idera Lawal:** performed the experiments on the guinea pig skin, did the experiments on the porcine cadavers and excised the skin from the cadavers. **Andrew Le Blanc:** performed the experiments on the guinea pig skin. **Veronica O'Brien:** performed the experiments on the human skin. **Cormak Weeks:** did the experiments on the porcine cadavers and excised the skin from the cadavers. **Whitney Tran:** performed the experiments on the human skin. **Yatish Rane:** contributed in experiments on the GP skin with 2 kg normal static load. **Emil Khusnatdinov:** did the experiments on the porcine cadavers and excised the skin from the cadavers. **Jeremy Marston:** Writing - review & editing, conceived the project and designed the experiments, Final editing was done.

Declaration of competing interest

All the authors declare no competing interests.

Acknowledgments

We would like to thank the Department of Animal Sciences at Texas Tech for porcine cadavers. This work was financially supported by The National Science Foundation via award CBET-1749382. We also thank Inovio Pharmaceuticals for providing the injector devices.

Appendix A. Supplementary data

Supplementary data to this article can be found online at https://doi.org/10.1016/j.jddst.2020.102043.

References

[1] Joy Schramm, Samir Mitragotri, Transdermal drug delivery by jet injectors: energetics of jet formation and penetration, Pharmaceut. Res. 19 (11) (2002) 1673–1679, https://doi.org/10.1023/A:1020753329492.

[2] Andrew Taberner, N Catherine Hogan, Ian W. Hunter, Needle-free jet injection using real-time controlled linear lorentz-force actuators, Med. Eng. Phys. 34 (9) (2012) 1228–1235, https://doi.org/10.1016/j.medengphy.2011.12.010.
[3] M. Moradiafrapoli, J.O. Marston, High-speed video investigation of jet dynamics from narrow orifices for needle-free injection, Chem. Eng. Res. Des. 117 (2017) 110–121, https://doi.org/10.1016/j.cherd.2016.10.023.
[4] Jeanne C. Stachowiak, Marcio G. von Muhlen, Thomas H. Li, Laleh Jalilian, Sapun H. Parekh, Daniel A. Fletcher, Piezoelectric control of needle-free transdermal drug delivery, J. Contr. Release 124 (1–2) (2007) 88–97, https://doi.org/10.1016/j.jconrel.2007.08.017.
[5] Hiroshi Miyazaki, Shingo Atobe, Takamasa Suzuki, Hiromitsu Iga, Kazuhiro Terai, Development of pyro-drive jet injector with controllable jet pressure, J. Pharmaceut. Sci. 108 (7) (2019) 2415–2420, https://doi.org/10.1016/j.xphs.2019.02.021.
[6] Yoshiyuki Tagawa, Nikolai Oudalov, A. El Ghalbzouri, Chao Sun, Detlef Lohse, Needle-free injection into skin and soft matter with highly focused microjets, Lab Chip 13 (7) (2013) 1357–1363, https://doi.org/10.1039/C2LC41204G.
[7] Akihito Kiyama, Nanami Endo, Sennosuke Kawamoto, Chihiro Katsuta, Kumiko Oida, Akane Tanaka, Yoshiyuki Tagawa, Visualization of penetration of a high-speed focused microjet into gel and animal skin, J. Visual 22 (3) (2019) 449–457, https://doi.org/10.1007/s12650-019-00547-8.
[8] U. Schneider, R. Birnbacher, E. Schober, Painfulness of needle and jet injection in children with diabetes mellitus, Eur. J. Pediatr. 153 (6) (1994) 409–410, https://doi.org/10.1007/BF01983402.
[9] Samir Mitragotri, Current status and future prospects of needle-free liquid jet injectors, Nat. Rev. Drug Discov. 5 (7) (2006) 543–548, https://doi.org/10.1038/nrd2076.
[10] Harvinder S. Gill, Mark R. Prausnitz, Coated microneedles for transdermal delivery, J. Contr. Release 117 (2) (2007) 227–237, https://doi.org/10.1016/j.jconrel.2006.10.017.
[11] Katharina Cu, Ruchi Bansal, Samir Mitragotri, David Fernandez Rivas, Delivery strategies for skin: comparison of nanoliter jets, needles and topical solutions, Ann. Biomed. Eng. (2019) 1–12, https://doi.org/10.1007/s10439-019-02383-1.
[12] Yogeshvar N. Kalia, Aarti Naik, James Garrison, Richard H. Guy, Iontophoretic drug delivery, Adv. Drug Deliv. Rev. 56 (5) (2004) 619–658, https://doi.org/10.1016/j.addr.2003.10.026.
[13] Anubhav Arora, Liquid and powder jet injectors in drug delivery: mechanisms, designs, and applications, in: Nina Dragicevic, Howard I. Maibach (Eds.), Percutaneous Penetration Enhancers Physical Methods in Penetration Enhancement, Springer Berlin Heidelberg, Berlin, Heidelberg, 2017, pp. 221–230, https://doi.org/10.1007/978-3-662-53273-7_14.
[14] Anubhav Arora, Mark R. Prausnitz, Samir Mitragotri, Micro-scale devices for transdermal drug delivery, Int. J. Pharm. 364 (2) (2008) 227–236, https://doi.org/10.1016/j.ijpharm.2008.08.032.
[15] S Paudel Kalpana, Mikolaj Milewski, Courtney L. Swadley, Nicole K. Brogden, Priyanka Ghosh, Audra L. Stinchcomb, Challenges and opportunities in dermal/transdermal delivery, Ther. Deliv. 1 (1) (2010) 109–131, https://doi.org/10.4155/tde.10.16.
[16] Jingjing Jiang, Stephanie J. Ramos, Preeti Bangalore, Paul Fisher, Kristine Germar, Brian K. Lee, Dan Williamson, Andrea Kemme, Eric Schade, Jay McCoy, Kar Muthumani, David B. Weiner, Laurent M. Humeau, Kate E. Broderick, Integration of needle-free jet injection with advanced electroporation delivery enhances the magnitude, kinetics, and persistence of engineered dna vaccine induced immune responses, Vaccine 37 (29) (2019) 3832–3839, https://doi.org/10.1016/j.vaccine.2019.05.054.
[17] Barney S. Graham, Mary E. Enama, Martha C. Nason, Ingelise J. Gordon, Sheila A. Peel, Julie E. Ledgerwood, Sarah A. Plummer, John R. Mascola, Robert T. Bailer, Mario Roederer, et al., Dna vaccine delivered by a needle-free injection device improves potency of priming for antibody and cd8+ t-cell responses after rad5 boost in a randomized clinical trial, PLoS One 8 (4) (2013), https://doi.org/10.1371/journal.pone.0059340.
[18] James W. McKeage, Bryan P. Ruddy, Poul MF. Nielsen, Andrew J. Taberner, The effect of jet speed on large volume jet injection, J. Contr. Release 280 (2018) 51–57, https://doi.org/10.1016/j.jconrel.2018.04.054.
[19] James W. McKeage, Bryan P. Ruddy, Poul MF. Nielsen, Andrew J. Taberner, Power-efficient controlled jet injection using a compound ampoule, J. Contr. Release 291 (2018) 127–134, https://doi.org/10.1016/j.jconrel.2018.10.025.
[20] Pankaj Rohilla, Yatish S. Rane, Idera Lawal, Andrew Le Blanc, Justin Davis, James B. Thomas, Cormak Weeks, Whitney Tran, Paul Fisher, Kate E Broderick, et al., Characterization of jets for impulsively-started needle-free jet injectors: influence of fluid properties, J. Drug Deliv. Sci. Technol. 53 (2019) 101167, https://doi.org/10.1016/j.jddst.2019.101167.
[21] Jonathan A. Simmons, Justin Davis, Thomas James, Juan Lopez, Andrew Le Blanc, Haley Allison, Haley Slook, Paul Lewis, Joshua Holtz, Paul Fisher, et al., Characterization of skin blebs from intradermal jet injection: ex-vivo studies, J. Contr. Release (2019), https://doi.org/10.1016/j.jconrel.2019.06.032.
[22] Nickolas P. Demas, Ian W. Hunter, An electronic force sensor for medical jet injection, J. Med. Dev. Trans. ASME 13 (2) (2019), https://doi.org/10.1115/1.4043196.
[23] Pragun Goyal, Nikola Kojic, Needle-free injection guide, US Patent (April 21 2020), 10,625,020.
[24] R.A. Hingson, J.G. Hughes, Clinical studies with jet injection; a new method of drug administration, Curr. Res. Anesth. Analg. 26 (6) (1947) 221–230.
[25] Ali Jafer Mohammed, Salah AlAwaidy, Shyam Bawikar, Padmamohan J. Kurup, Emadaldin Elamir, Mahmoud MA. Shaban, Sharif M. Sharif, Harrie Gam van der Avoort, Mark A. Pallansch, Pradeep Malankar, et al., Fractional doses of inactivated poliovirus vaccine in Oman, N. Engl. J. Med. 362 (25) (2010) 2351–2359, https://doi.org/10.1056/NEJMoa0909383.
[26] Cormac Flynn, Andrew Taberner, Poul Nielsen, Measurement of the force–displacement response of in vivo human skin under a rich set of deformations, Med. Eng. Phys. 33 (5) (2011) 610–619, https://doi.org/10.1016/j.medengphy.2010.12.017.
[27] Chris Cappello, Wixey Matt, John W. Bingham, Needle-free intradermal injection device, US Patent 10 (June 18 2019), 322,238.
[28] Torben Hansen, Nozzle device with skin stretching means, US Patent App (January 25 2007), 11/453,575.
[29] Brent E. Vecchia, Annette L. Bunge, Animal models: a comparison of permeability coefficients for excised skin, in: Dermal Absorption Models in Toxicology and Pharmacology, CRC Press, 2005, p. 305, https://doi.org/10.1201/9780203020821.ch15.
[30] S.A. Ranamukhaarachchi, S. Lehnert, S.L. Ranamukhaarachchi, L. Sprenger, T. Schneider, I. Mansoor, K. Rai, U.O. Häfeli, B. Stoeber, A micromechanical comparison of human and porcine skin before and after preservation by freezing for medical device development, Sci. Rep. 6 (2016) 32074, https://doi.org/10.1038/srep32074.
[31] Jeremy O. Marston, Carla MR. Lacerda, Characterization of jet injection efficiency with mouse cadavers, J. Contr. Release 305 (2019) 101–109, https://doi.org/10.1016/j.jconrel.2019.05.023.
[32] Hamed Joodaki, Matthew B. Panzer, Skin mechanical properties and modeling: a review, Proc. IME H J. Eng. Med. 232 (4) (2018) 323–343, https://doi.org/10.1177/0954411918759801.
[33] Pankaj Rohilla, Jeremy O. Marston, In-vitro studies of jet injections, Int. J. Pharm. 568 (2019) 118503, https://doi.org/10.1016/j.ijpharm.2019.118503.
[34] J. Ankersen, A.E. Birkbeck, R.D. Thomson, P. Vanezis, Puncture resistance and tensile strength of skin simulants, Proc. IME H J. Eng. Med. 213 (6) (1999) 493–501, https://doi.org/10.1243/0954411991535103.
[35] Iman Mansoor, Jacqueline Lai, Sahan Ranamukhaarachchi, Veronika Schmitt, Dana Lambert, Dutz Jan, Urs O. Häfeli, Boris Stoeber, A microneedle-based method for the characterization of diffusion in skin tissue using doxorubicin as a model drug, Biomed. Microdevices 17 (3) (2015) 61, https://doi.org/10.1007/s10544-015-9967-4.
[36] Satsue Hagisawa, Tatsuo Shimada, Skin morphology and its mechanical properties associated with loading, in: Pressure Ulcer Research, Springer, 2005, pp. 161–185, https://doi.org/10.1007/3-540-28804-X_11.
[37] Fouad Khatyr, Imberdis Claude, Vescovo Paul, Daniel Varchon, Jean-Michel Lagarde, Model of the viscoelastic behaviour of skin in vivo and study of anisotropy, Skin Res. Technol. 10 (2) (2004) 96–103, https://doi.org/10.1111/j.1600-0846.2004.00057.x.
[38] C. Pailler-Mattei, S. Bec, H. Zahouani, In vivo measurements of the elastic mechanical properties of human skin by indentation tests, Med. Eng. Phys. 30 (5) (2008) 599–606, https://doi.org/10.1016/j.medengphy.2007.06.011.
[39] John Z. Wu, G Dong Ren, W.P. Smutz, A.W. Schopper, Modeling of time-dependent force response of fingertip to dynamic loading, J. Biomech. 36 (3) (2003) 383–392, https://doi.org/10.1016/S0021-9290(02)00427-X.
[40] Barry Goldstein, Joan Sanders, Skin response to repetitive mechanical stress: a new experimental model in pig, Arch. Phys. Med. Rehabil. 79 (3) (1998) 265–272, https://doi.org/10.1016/S0003-9993(98)90005-3.
[41] Catherine Escoffier, Jean de Rigal, Annie Rochefort, Régis Vasselet, Jean Luc Lévêque, G. Pierre, Agache, Age-related mechanical properties of human skin: an in vivo study, J. Invest. Dermatol. 93 (3) (sep 1989) 353–357, https://doi.org/10.1016/0022-202X(89)90058-4.
[42] Bruce J. Sangeorzan, Richard M. Harrington, Craig R Wyss, Joseph M. Czerniecki, Frederick A. Matsen III, Circulatory and mechanical response of skin to loading, J. Orthop. Res. 7 (3) (1989) 425–431, https://doi.org/10.1002/jor.1100070315.